An open-source workflow for open-cell foams modelling: geometry generation and CFD simulations for momentum and mass transport

An open-source workflow for open-cell foams modelling: geometry generation and CFD simulations for momentum and mass transport

Enrico Agostini[a], Gianluca Boccardo[1,a], Daniele Marchisio[a]

[a]*Department of Applied Science and Technology, Institute of Chemical Engineering, Politecnico di Torino, Corso Duca degli Abruzzi, 24, 10129, Torino, Italy*

Abstract

Open-cell foams are porous materials characterized by high porosity and large specific surface, industrially employed as catalyst supports or particulate filters. These materials can be modelled using periodic lattices, or with more complex approaches based on Voronoi tessellations. This work introduces, tests, and makes available an open-source workflow (Agostini (2021)) based on `Blender` that can reproduce great varieties of geometries with a limited cost for their modeling. An example of the exploration capabilities of this workflow is presented in the form of CFD simulations for flow field and mass transfer (performed with OpenFOAM) on the created geometries, eventually obtaining an effective particle deposition/filtration coefficient K_d. The results are interpreted using constitutive equations and other functional forms depending on geometric parameters which prove to be insufficient in explaining the variations in filtration performance, highlighting the need for more detailed exploration, the objective for which this workflow was developed.

Keywords: Open-cell foams, CFD, Open-source, `Blender`, `OpenFOAM`

2010 MSC: 00-01, 99-00

1. Introduction

The interest of the process industry towards porous materials, such as open-cell solid foams, has greatly increased over the last twenty years. The reasons

*Corresponding author

Email address: `gianluca.boccardo@polito.it` (Gianluca Boccardo)

reside in their unique properties such as mechanical resistance, very high porosity, which results in lower pressure drops compared to other packing media, large specific surface area and high thermal conductivity, which are important factors for mass and heat transfer. The production process often begins with polyurethane foams, which are usually used as precursor for ceramic or metallic ones (Twigg and Richardson, 2007).

They are produced by inflating a gas, usually air, into molten polymer and inducing polymerization. A good example of the dynamic of polymeric foam formation process can be found in Karimi et al. (2017). The polymeric structures obtained are then impregnated by ceramic pastes/slurries or metallic powders, together with wetting and binding agents. Finally these wet foams are calcinated, obtaining a *positive* replica of the polyurethane foams. The foams thus obtained have the peculiarity of presenting hollow ligaments, due to the destruction of the polymeric foam inside. Many other techniques have been developed in the last twenty or more years, such as direct blowing of melted metal alloys or metallic powders sintering, as reported by Singh and Bhatnagar (2018). Notable uses of ceramic foams are: molten metal filters, monolithic catalyst supports (Richardson et al., 2003), soot filters (Meloni et al., 2019), column packing for packed bed reactors Wehinger et al. (2019). Metallic foams are commonly used as filters, catalyst supports or reactor and heat exchanger packings due to their great performaces in heat transfer applications. Despite the great advancements in the production techniques developed in the last 30 years, the optimization of such materials remain a challenging issue. The main parameters used for their characterization are porosity and the number of *pores per inch* (ppi), which indicate the average pore diameter, but they do not give any clue regarding important values such as the specific surface area S_V, used in the design of industrial devices or processes to estimate the heat exchange coefficient h or the pressure drops $\Delta P/L$. The optimization of such structures for different uses remains an open problem. In order to achieve this, it is crucial to develop an accurate theoretical model which can help in the evaluation of parameters such as porosity or specific surface area, important for the final

foam performance. This would allow a better understanding and a more accurate estimation of the transport processes occurring inside this type of porous materials.

The first attempts to properly model the geometric structure of open-cell foams relied on ideal periodic geometries. Such structures are ideal convex polyhedra, with regular polygonal faces, which can perfectly fill the space in a repetitive fashion, forming a structure with congruent repetitive cells. The advantage of using such geometries resides in the fact that analytical correlations can be derived to describe the geometrical structure, such as edges length, area of the cell windows and the volume of the pores. This also allows to an easier estimation of the resulting porosity and specific surface. Common polyhedra with such properties are cubes, dodecahedra and truncated octahedra (also known as *tetrakaidecahedron*).

Lord Kelvin (Thomson et al., 1887) proposed it as the shape which attained the minimal surface tension in a foam made of bubble of equal size. This structure, better known as *Kelvin's cell*, has 14 faces (6 squares and 8 hexagons) and 36 edges of equal size. This polyhedron is still widely considered the ideal shape that a solid foam cell would attain if the structure would be allowed to reach equilibrium during the synthesis process. Many authors used the Kelvin's Cell as a geometric model in their investigation of transport phenomena inside porous open-cell foams. In their review on solid foams and their application in the process industry Twigg and Richardson (2007) reported analytical correlations for the estimation of the specific surface S_V, pressure drops $\Delta P/L$ and heat transfer coefficient h, based on the Kelvin's cell geometry. Lacroix et al. (2007) validated a cubic cell model with pressure drop measurements. Sullivan et al. (2008), proposed a general geometric model based on the tetrakaidecahedron reporting several parametric correlation to describe such geometrical structure based on the edge length L, varying the aspect ratio of the cell. Incera Garrido et al. (2008) proposed mass transfer and pressure drops correlations based both on experimental measurements and analysis of the geometry obtained with an MRI technique, highlighting the influence of the pore size and porosity. Inayat

et al. (2011a), Inayat et al. (2011c), Inayat et al. (2011b) developed analytical geometrical correlations based on the Kelvin's Cell model comparing them to data obtained by characterization of real foams with μ-CT tomography. Kumar and Topin (2014) used an analytical approach, based on the tetrakaidecahedron unit cell, to investigate the thermohydraulic aspects (pressure drops and thermal conductivity) of several different foams structure, comparing a large amount of experimental results found in literature. Ambrosetti et al. (2017) developed a very detailed analytical model, based on the Kelvin's unit cell, and validated it with a large amount of experimental data. Della Torre et al. (2016) used the Kelvin's Cell model for numerical simulations of a catalytic reaction in open-cell foams substrates.

Along with analytical models, in the last 20 years many authors used numerical methods to study and characterize these materials. Krishnan et al. (2006) studied fluid flow and pressure drops with DNS methods. Lucci et al. (2014), Lucci et al. (2015) and Lucci et al. (2017) studied momentum, heat, mass transfer and catalytic reactions using a regular and a randomized Kelvin's cell model coupled with CFD. For the same geometrical model Della Torre et al. (2014) explored the flow field over different fluid dynamic regimes. Das et al. (2016), Das et al. (2017), Chandra et al. (2019) studied momentum and mass transfer inside a periodic Kelvin's cell using CFD with an *Immersed Boundary Method*. However, it is well reported that not all the important properties of the open-cell foams can be caught by simulations over ordered lattice, as for instance reported by Habisreuther et al. (2009) , thus along the simplified analytical Tetrakaidecahedron models many authors focused their research on developing more realistic models, in order to better describe the with random nature of open-cell foams. Lautensack et al. (2008), Redenbach (2009), Wejrzanowski et al. (2013), were between the first to proposed the use of random tessellations as an optimal model to represent the cellular random nature of solid foams. Random Voronoi or Voronoi-Laguerre algorithms subdivide the space into regions, which can be taken to represent the pores of a real foam. The advantage of this approach lies in the fact that a large range of parameters

affecting the final geometry can be explored. This allows the creation and the study of many structures and configurations that wouldn't otherwise be possible to experimentally investigate. Many authors, such as Bracconi et al. (2017), Nie et al. (2017a), Nie et al. (2017b), Das et al. (2018) used random tessellations to generate geometries and investigated transport phenomena using numerical simulations.

Different algorithms and software were used by these authors to create the geometries: `LIGGGHTS` (Kloss et al., 2012) or `LAMMPS` to compute the initial random seeds of the tessellation, `voro++` (Rycroft, 2009) to compute the tessellations and `Surface Evolver` (Brakke, 1992) to create the superficial mesh.

Most of the aforementioned software can produce very good results, however, to the best of the authors' knowledge, there is no example in literature of any open-source tools which fit in a unique platform the geometry generation and the transport simulation workflow, for the modeling of this kind of foams. Therefore, the objective of this work is to introduce, test and validate an open and flexible *in-silico* tool, that would be able to reproduce a great variety of structures, exploring large parameter ranges, in order to be able to optimize the geometric structure according to the different application areas. The innovative tool presented in this work will rely only on the open-source computer graphics code `Blender` and on `Python` programming language code to calculate and create the final geometry. The initial set of random points would be generated by a random sphere packing (either mono- or poly-dispersed), following an already validated workflow proposed by Boccardo et al. (2015). The position of the edges and nodes of the tessellation, generated from the starting random seeds, is retrieved from the Voronoi algorithm. Then `Blender` creates cylinders and sphere at the supplied coordinates to generate the foam structure. The resulting geometry will be used to define a computational domain in which to run CFD simulations in the `OpenFOAM` environment.

First, the flow field would be calculated, to estimate the pressure drop and hydraulic permeability of the generated geometries. Then, micro-scale mass transfer simulations would be carried out to explore transport and surface reac-

tion/deposition of colloidal particles through these porous media. This problem is of great importance in chemical and environmental engineering, and as such it has been investigated by many authors dealing with a variety of applications, such as particle deposition in filtration (Yao et al., 1971), catalytic processes through filter beds in the automotive industry (Bensaid et al. 2010), aquifers remediation (Tosco et al., 2012) and filtration and adsorption of pollutants in structured ceramics König et al. (2020) , to cite a few. A thorough research of the relevant literature yielded no related articles on this topic applied to open-cell foams. This work will focus on phenomena of fast deposition/reaction of colloidal particles on the solid surface. This circumstance usually occurs either in the event of clean-bed filtration Yao et al. (1971) or in case of a very fast catalytic reaction, whose coefficient of reaction tends to infinity. In this particular cases deposition is driven by Brownian motion and steric interception mechanisms. Following the model and methodology proposed by Boccardo et al. (2014) and Boccardo et al. (2018), and then used in subsequent works Marcato et al. (2021); Crevacore et al. (2016), the results of the scalar transport simulations will be used to calculate an effective macroscopic particle deposition rate coefficient K_d, which would be used to estimate the efficiency of clean-bed filtration of open-cell foams. As an aside, it has to be noted that this framework and some of the results presented can be readily extended for heat transfer problems. In those cases, however, the heat conduction in the solid needs to be upscaled with appropriate non-equilibrium transfer terms, as demonstrated by Municchi and Icardi (2020a).

2. Workflow description and theoretical background

The creation of foam-like geometries is a complex process involving several steps and touching different fields in computational geometry. To reproduce the cellular structures of solid foams, the space is subdivided into regions or *cells*, using a Voronoi tessellation or similar kinds of geometrical algorithms. The starting points for this subdivision, called *seeds*, are provided by the centers of

a random packing of spheres inside a confined space. The advantage of using this workflow is that the resulting foam properties can be linked to the initial parameters of the geometric model. Consequently, properties such as porosity ε, specific surface S_V, and permeability k can be estimated more rigorously.

The open-source computer graphics software `Blender` is used both for performing the rigid body simulation, resulting in the sphere packing, and to generate the geometry in the form of a `.stl` file. Subsequently, used as a basis to build the computational domain of the system, which is then meshed using the open-source CFD code `OpenFOAM`, also used to carry out the numerical simulations.

In Section 2.1 an overview of the Kelvin's Cell ideal model is presented. In Section 2.2 the creation of the spheres packing is reviewed. Then, the tessellation process is treated in Section 2.3. In Section 2.4 the geometry model and his creation is presented. Finally, in Section 2.5 the computational methods are presented.

2.1. Ideal model: the Kelvin Cell

An ideal approach to the modeling of open-cell foams is the Kelvin Cell model. It was first proposed by Lord Kelvin as the arrangement taken by bubbles in the formation of liquid foams because it is the configuration with minimal surface tension. It consists of a *tetrakaidecahedron*, an ideal polyhedron, with 14 faces, 36 edges and periodic in space. Its representative elementary volume (REV), the cell itself, is frequently used to model open-cell foams because of its shape simplicity, easily apparent connectivity and periodicity. Its features are also used as comparison in the analysis of random generated geometries, to assess how closely this structure resemble ideal shapes.

2.2. Sphere packing process

As already mentioned in the introduction section, modeling open-cell foams by means of ordered lattice shapes such as the Kelvin Cell is not sufficient to catch some of their important properties and therefore other approaches were conceived in order to cope with the higher level of complexity. Among these

the use of random Voronoi tessellation is preferred because they show comparable randomness. The structures resulting from this algorithm can be used as a skeleton for the final foam model. The initial parameters of the tessellation, namely the shape of the distribution of spheres which gives the initial random seeds, can be tuned to create different structures varying the resulting randomness. The creation of a mono-disperse or a poly-disperse hard-sphere packing is carried out using the open-source code `BSand`. As reported by Boccardo et al. (2015), the computer graphics code `Blender` solves the Newton's equation of motion for system constituted of N particles. The dynamics of collisions of a system of N rigid-body spheres is solved by means of the Bullet Physics Library (BPL). This collection of codes provides several iterative algorithms to simulate the packing process of a large number of elements in a robust and accurate way, in a relatively low computational time. The geometrical input parameters to be set are: the container shape, its size, and the hard-spheres size distribution main parameters. For the generation of the random sphere packings of the present work, the grain size distribution chosen is Gaussian. A random variable X is normally distributed when its associated probability density function is:

$$f_X(x) = \frac{1}{\sigma\sqrt{2\pi}} \exp\left(-\frac{1}{2}\frac{(x-\mu)^2}{\sigma^2}\right) \tag{1}$$

$$CV(x) = \frac{\sigma}{\mu} \tag{2}$$

where μ and σ are respectively the mean value and the standard deviation of the random variable. For such distribution one can define the coefficient of variation $CV(x)$, reported in Eq. (2), the ratio between the standard deviation and the mean value of the distribution. Such coefficient, together with the mean sphere diameter μ are the input parameters provided to `Blender`, by means of `python` code, to compute the sphere packing. Finally, the locations and dimensions of each sphere inside the container are retrieved.

2.3. Computation of tessellation

A three-dimensional tessellation (which can be arranged as random) is a subdivision of space into polyhedra, which share boundaries with their neighbours not overlapping one another.

2.3.1. Voronoi and Laguerre tessellations

The Voronoi Diagram is a well known type of random tessellation which, starting from an initial set of point, the *seeds*, subdivide space into convex polyhedra in such a way that the region around a seed consists of all the points closer to that seed than to any other. More rigorously, given a starting set of N random seeds $S = \{P_1, P_2, ..., P_n\} \subset \mathbb{R}^3$ and considering a generic point $\boldsymbol{x} \in \mathbb{R}^3$, being $d(\boldsymbol{x}, P_i)$ the Euclidean distance, a generic Voronoi region $\mathrm{R}(\boldsymbol{x}, P_i)$ is defined by

$$R(\boldsymbol{x}, P_i) = \{\boldsymbol{x} \in \mathbb{R}^3 \mid d(\mathbf{x}, P_i) < d(\mathbf{x}, P_j),\ j \neq i\} \tag{3}$$

Power Diagrams are another important type of cellular-like geometric structures. They are a generalization of a Voronoi tessellation, introducing a weighing factor $w(P_i)$ to the initial seeds, as reported in Aurenhammer (1987). In particular, the Laguerre-Voronoi tessellation is a second order Power Diagram whose weighing factors are the square of the radii r_i of the spheres centered in the initial set of seeds $S = \{P_1, P_2, ..., P_n\} \subset \mathbb{R}^3$, resulting in Eq. (4):

$$R(\boldsymbol{x}, P_i) = \{\boldsymbol{x} \in \mathbb{R}^3 \mid d(\mathbf{x}, P_i) - r_i^2 \ <\ d(\mathbf{x}, P_j) - r_j^2,\ j \neq i\} \tag{4}$$

The use of a mono-disperse set of spheres combined with a Voronoi tessellation results in a structure with regular-shaped and homogeneous cells, resembling the ideal structure of the Kelvin's Cell. This kind of structure is attained whenever the foam creation process allows the structure to reach the *mechanical equilibrium*. However, most production processes result in foams with irregular-shaped and widely heterogeneous cells. The use of the Laguerre-Voronoi tessellation coupled with poly-disperse spheres packing, together with a wise choice of

the cells volume distribution, can result in more realistic geometrical structures, able to better describe the phenomena occurring in such materials.

2.3.2. The tessellation algorithm

The computation of the tessellation is carried out using the `python` module `Tess`, developed by Smith (2019), which has the Python bindings to the C++ code `voro++`, developed by Rycroft (2009), a software library which carries out three-dimensional Voronoi and Laguerre-Voronoi tessellations. This code carries out cell-based calculations, storing all the outputs in the *class* `tess.Cell`, which contains information regarding vertices and centroids locations, facets connectivity and neighbour cells, to cite a few. The input parameters are the initial *seeds* coordinates and the *bounding box* coordinates; in the case of Laguerre-Voronoi diagrams the spheres radii acting as the tessellation algorithm weights. Additionally, the code can compute a periodic or non-periodic diagram, by enabling or disabling a Boolean parameter. The output is in the form of a list of instances of the `Cell` class, each corresponding to the convex polyhedron computed starting from the initial sphere packing. An additional feature to compute and list each edge by its vertices was added, both for singular cells and the global structure, inspired by the code developed by Gostik (2017). Finally, a list of all the edges is computed (purged of all the duplicates) containing the arrays of the coordinates of each pair of vertices defining an edge. Then, this list can be safely passed as input to the next step of the workflow which generates the geometry file.

2.4. Geometry model and creation

The geometry creation is carried out by the open-source software `Blender`, which takes as input the edges coordinates previously computed. The output is a `.stl` file which is then ready to be meshed and used as input for the CFD code.

Ball-and-sticks model. The simplest model to be generated is the so called ball-and-sticks model, in which the struts are simple circular or triangular cylinders

and the nodes are spheres. The input parameters are the spheres and cylinders diameter and the edges coordinates. The code store the latter in a class, conveniently called `Edges`, whose *methods* compute the length of the cylinder and the rotations with respect to the y- and z-direction, namely θ and ϕ angles.

2.5. CFD simulations

The meshing process and numerical simulations are carried out within the `OpenFOAM` environment, an open-source finite-volume CFD code. The computational domain previously created is chosen to represent a microscopic portion of a foam pellet. Although the characteristic length of the pores is very small, at the order of hundreds of µm, the continuum hypothesis still holds true. The transport phenomena inside the pores are governed by the Continuity equation, which describe the mass balance in the system and the Navier-Stokes equation, which describes the momentum balance. For an incompressible fluid, flowing within the void fraction of the geometry with constant density and viscosity, these equations read as follows:

$$\frac{\partial U_i}{\partial x_i} = 0 \tag{5}$$

$$\frac{\partial U_i}{\partial t} + U_j \frac{\partial U_i}{\partial x_i} = -\frac{1}{\rho}\frac{\partial p}{\partial x_i} + \nu \frac{\partial^2 U_i}{\partial x_j^2} \tag{6}$$

where U_i is the i-th component of the fluid velocity, p is the fluid pressure, ρ and ν are respectively the fluid density and the kinematic viscosity. The results of the simulations are then interpreted according to macro-scale continuum equations for fluid flows in porous media. The parameters of these spatially *smoothed* equations (e.g., porosity and permeability) result from averaging procedures that are carried out over the microscopic governing equations on both the porous media and the fluid flow, as explained by Whitaker (2013) and also reported in Icardi et al. (2014).

Thus, Eq. (5) and Eq. (6) become, respectively:

$$\frac{\partial V_i}{\partial x_i} = 0 \tag{7}$$

$$\frac{\partial V_i}{\partial t} + V_j \left(\varepsilon \frac{\partial V_i}{\partial x_i} \right) = -\frac{1}{\rho} \frac{\partial p}{\partial x_i} + g_i + \gamma V_i \tag{8}$$

where V_i is the Darcy velocity (or superficial velocity) in the porous medium, ε is the medium porosity. The friction coefficient γ can be expressed as $\gamma = \mu/\rho k$, where k is the foam permeability and μ is the fluid viscosity. If the flow is stationary, in laminar regime, and gravity effects are unimportant, some terms in Eq. (8) can be neglected, thus obtaining Darcy's Law. For conciseness, this can be written in a one-dimensional expression (along the main flow direction), resulting in the well-known form:

$$\frac{\Delta P}{L} = -\frac{\mu |V|}{k} \tag{9}$$

where $\Delta P/L$ is the pressure drop per unit volume. For conditions in which the inertial forces are more significant ($\mathrm{Re} > 1 - 10$), even if the flow is not fully turbulent, an additional term dependent on the superficial velocity V can be added to the friction factor, which becomes $\gamma = \mu/\rho k + \beta |V|$. Substituting in Eq. (7) as before, this yields the Forchheimer's Equation:

$$\frac{\Delta P}{L} = -\frac{\mu |V|}{k_1} - \frac{\rho |V|^2}{k_1} \tag{10}$$

where $k_1 = 1/\beta$ is the inertial permeability.

At the microscopic scale, the transport of solutes can be described by a linear advection-diffusion-reaction equation:

$$\frac{\partial c}{\partial t} + \frac{\partial}{\partial x_i} \left(U_i c \right) - \frac{\partial}{\partial x_i} \left(\mathcal{D} \frac{\partial c}{\partial x_i} \right) = k_b c \ \text{ on } \ \Omega_b \subset \Omega \subset \mathbb{R}^3 \tag{11}$$

with Ω_b the volume of fluid, Ω the total volume, c is the scalar concentration (mol m^{-3}), U is the pore-scale velocity (m s^{-1}), which can be obtained by Eq. (6), $\mathcal{D}$ the molecular diffusion (m^2 s^{-1}) and k_b is the bulk reaction coefficient (s^{-1}). This equation can be used to model the transport of colloidal particles under

the assumption of a dilute system and negligible particle Stokes number: most importantly for particles of sufficiently small dimension. The latter meaning that the size of the particles is much smaller than the characteristic flow scale and collector size ($d_p/d_c \approx 10^{-3}$) (Boccardo et al., 2018). An homogeneous Dirichlet boundary condition $c = 0$ is chosen to model the deposition of particles on the solid surface, meaning that all the colloids impacting on the walls of the collector are captured. Boccardo et al. (2018) derived an expression for an effective particle deposition rate K_d, applying to Eq. (11) a volume averaging operator, under the steady-state condition and sole superficial reaction, resulting in:

$$K_d = \frac{F_{tot}^{in}(c) - F_{tot}^{out}(c)}{|\Omega|\langle c \rangle} \tag{12}$$

where the numerator represents the total effective flux of the scalar c through the system, $\langle c \rangle$ is the average scalar concentration and $|\Omega|$ is the total volume of the system. Finally it would be useful to introduce an *advective* Damköhler number Da defined as:

$$\mathrm{Da} = \frac{K_d \cdot d_{pore}}{V} \tag{13}$$

where K_d is the deposition rate previously defined, V is the superficial velocity and d_{pore} the diameter of the mean pore of the foam.

3. Test cases and numerical details

The current section will describe the different test cases explored for this work, along with the operating conditions and numerical details of the simulations. The generation of the geometry will be described first, then the meshing strategy, and finally the simulations setup. All the technical information regarding hardware and computational times are reported in the Supporting information available with this article.

Geometry model generation. The geometrical model explored for this work are of two types: the Kelvin's Cell simplified model (a truncated octahedron), and structures originated from random tessellation, in particular Voronoi and Laguerre-Voronoi tessellation. For each type of geometry four values of *pore per inch* (PPI) have been considered, namely PPI $= \{10, 20, 30, 45\}$, and five values of porosity ε, namely $\varepsilon = \{0.77, 0.79, 0.85, 0.89, 0.95\}$, for a total of 20 cases. The Kelvin's Cell geometry creation is straightforward, since all vertices positions are permutations of $(0, \pm\sqrt{2}/2, \pm\sqrt{2})$, resulting in a tetrakaidecahedron with edge length equal to 1. The connectivity between nodes is simply obtained from observing the figure and the edges are calculated as the vectors linking vertices. In the case of foams generated by random tessellation, the geometry aims instead to represent a small cubic portion belonging to the bulk of the real structure. First the random sphere packing is generated using the code `Bsand`, as reported in the previous section. In order to assure independence from any wall effects due to the container, a very large packing is generated with up to 6000 grains packed inside a cubic container with side dimension equal to 15 times the average grain diameter μ . This procedure, despite computationally burdensome, ensures random disposition of the spheres in the bulk part of the packing, whose resulting distance from the container walls is around 4 to 5 times mean grain diameters, as reported in Boccardo et al. (2015) and also ensure that the most inner part, which is the one from which the random seed are extracted, has dimension at least equivalent to five mean grain diameter. More details regarding the dimension of this part is given in Section 4.1 where the REV grid independence study is described. In the case of mono-disperse sphere packings, the grains are constituted by spheres with unitary diameter. In the case of poly-disperse packing, two different instances have been generated with same mean sphere volume $E(V)$, which is equal to the volume of sphere with unitary diameter, and two values of the coefficient of variation $CV(V)$, namely 0.2 and 0.35. Once the packings are generated, the coordinates and dimensions of the spheres are used to calculate the tessellation over a small cubic portion at the core of the volume. The two steps of this procedure are visualized in Fig. 1.

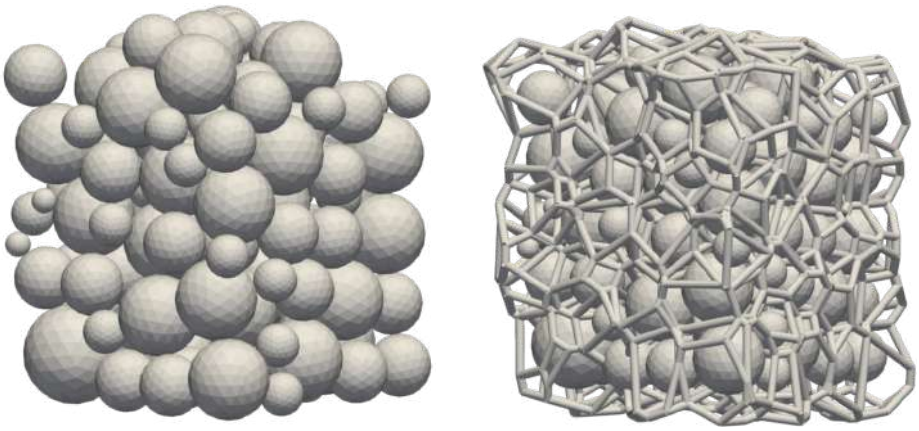

(a) Packed spheres (b) Resulting foam

Figure 1: Example of the two main steps in the creation of a foam REV. In (a) it is reported the original random sphere packing. In (b) the resulting open-cell foam, obtained with a periodic Laguerre-Voronoi algorithm, is reported overlapped to its generating sphere packing. Larger spheres have a larger area of influence, hence their resulting "cells" are much larger.

The dimension of this portion and its choice would be discussed in details in the next chapter. The output of the code is a collection of all the cell edges and nodes, in the form of point coordinates in space. The information regarding nodes and edges position and orientation are passed to `Blender`, via a `Python` script, which places cylinders and spheres in to reproduce struts and vertices.

In order to achieve the chosen pore density (PPI), the geometry file is scaled down, either using `Blender` or `OpenFOAM`, by a factor calculated as follow:

$$f_{scale} = \frac{\left(\frac{0.0254}{PPI}\right)}{D_{tess,mean}} \tag{14}$$

where the numerator is the pore size (in meters) of a foam having a certain PPI and the denominator is the mean cell size of the tessellation, calculated as the diameter of sphere having the same volume as the average cell. The strut diameter is chosen so as to reach the desired foam porosity, which is calculated from the computational volume mesh generated by `OpenFOAM`. By a trial-and-error procedure, a correlation between the strut dimension and the porosity ε has been derived.

Mesh generation. Once the foam geometry is generated it is exported in *.stl* format. An *.stl* file describe a solid volume by means of its surface, which is discretized by a triangulated mesh. This type of file formatting, being supported by a wide range of CAD/CAE software, is very common and portable. It is also the format of choice to define geometries to be meshed in `OpenFOAM`. The geometry exported from `Blender` represents the solid fraction of the domain, whereas the void/fluid fraction in-between is the part to be meshed by `OpenFOAM`. The meshing procedure is carried out in two main steps: first a *background* structured hexahedral mesh is generated by the `OpenFOAM` utility `blockMesh`. This hexahedral mesh is used as a starting point to build a *body-fitted* grid generated by the utility `snappyHexMesh`, also part of the `OpenFOAM` suite. The computational grids created in this manner are predominantly constituted by hexahedral cells, ensuring good numerical performance for the solver, and are then subsequently refined close to the solid walls, resulting in cells of increasing dimension moving farther away from the walls, towards the bulk of the fluid. This allows to have a large number of small cells in the areas where gradients are higher, whereas in the bulk of the fluid, where stresses are lower, the cell density is lower, thus reducing the total computational cost. The mesh generation process and the choice of optimal parameters are crucial steps in order to obtain a grid independent solution and an accurate representation of the original geometry. The strategy to achieve an accurate computational grid is to compromise between small initial background cells dimension, the refinement level and the amount of cells in each refinement layer. This is particularly true for geometrical structures such as open-cell foams, which have a void fraction ranging from 70% to well beyond 90%, meaning that a very large amount of cell is required to properly describe the fluid motion within the foam pores. In order to achieve solution grid independence, the mesh was progressively refined, both by decreasing the background cell dimension and increasing the refinement level on the solid surface. The comparison between the different meshes is carried out by confronting the values of porosity obtained as well as the solution of the flow field. For this work it has been determined that the optimal number of background cells per

pore diameter of around 22, the best refinement level value is $R = 2$, with 4 consecutive layers of refined cells from the solid surface. The details of the grid independence work would be shown in the next section.

Fluid flow simulations. As previously mentioned, the numerical simulations were carried out using the open-source CFD code `OpenFOAM 7`. The computational domain used in all the simulations carried out for this work has cubic shape with side L, with the origin of the axis at its center, with the diagonal vertices respectively x_{min}, y_{min}, $z_{min} = -L/2$ and x_{max}, y_{max}, $z_{max} = L/2$. The flow field is initialized by setting a fixed pressure difference $\Delta P/\rho$ in x-normal direction between the inlet and the outlet patches of the domain, which are x-normal surfaces with coordinates respectively $x_{Inlet} = -L/2$ and $x_{Outlet} = L/2$. The value of L is equal to the linear dimension of the REV (defined as a cubic volume), which in the case of the Kelvin Cell coincide with the cell itself, whereas for the random foam was determined with a study which is thoroughly explained in the next Chapter. This allows to have a fully developed flow field inside a small computational domain; although in this set-up there is no a-priori knowledge of the characteristic velocity of the system (and thus of the Reynolds number), it can be estimated using equation (9). A *no-slip* condition for the velocity U is applied at the solid surface of the foam, a condition of zero gradient at the outlet patch, whereas at the remaining sides of the domain a *symmetry* boundary conditions is applied, implying no fluid motion across those. The Newtonian incompressible fluid here considered is water, with density $\rho = 997.78$ kg m^{-3}, kinematic viscosity $\mu = 9.77 \times 10^{-4}$ kg m^{-1}s^{-1}. The system is solved using the solver `simpleFoam`, at a constant temperature $T = 293K$ (the energy equation was not solved) in steady-state condition, under laminar flow regime ($1 \cdot 10^{-4} < \mathrm{Re} < 1 \cdot 10^{-3}$). The Reynolds number for this work is defined as $\mathrm{Re} = U \cdot D_{pore}/\nu$, with D_{pore} being the mean pore diameter of the foam, defined as the diameter of a sphere having the same volume as the mean pore.

Scalar transport simulations. The results of the momentum transport simulations have been used for the mass transfer simulations solving Eq. (11), using the

same mesh. Five different operating conditions, for each combination of pore density and porosity, have been explored, changing the Pe number, namely $\mathrm{Pe} = \left\{5, 5\sqrt{10}, 50, 50\sqrt{10}, 500\right\}$, which was used to estimate the value of the diffusivity $\mathcal{D}$ from:

$$\mathcal{D} = \frac{U D_{pore}}{\mathrm{Pe}} \tag{15}$$

The system is solved at constant temperature, in steady-state condition using the solver `scalarTransportFoam`. The colloidal particles are represented by a scalar, acting as the normalized concentration, with an inlet value C_0 set equal to 1, a condition of zero gradientat the outlet patch and at the remaining sides of the domain a *symmetry* boundary condition is applied. On the solid walls a Dirichlet boundary condition, with a normalized concentration with a fixed value C_{walls} equal to 0, was imposed. The effective deposition rate coefficient K_d is estimated by the solver from the fluxes on the solid surfaces, using Eq. (12).

4. Results and discussion

In this section the results obtained from the numerical simulations will be presented. The first part will be dedicated to extensively comment the grid independence study, whereas in the second part the results obtained from the solution of the flow field and the particle deposition simulations will be discussed.

4.1. Grid independence study

The meshing procedure used during all the simulation campaign was presented in Chapter 3. The first goal of this study was to determine the optimal meshing strategy by tuning two parameters: the number of the starting `blockMesh` background cells and the level of refinement R performed by `snappyHexMesh` on the cells close to the solid surface.

In order to reduce the computational cost of such investigation, it was chosen to perform these simulations on the simplified Kelvin's Cell model, which is a

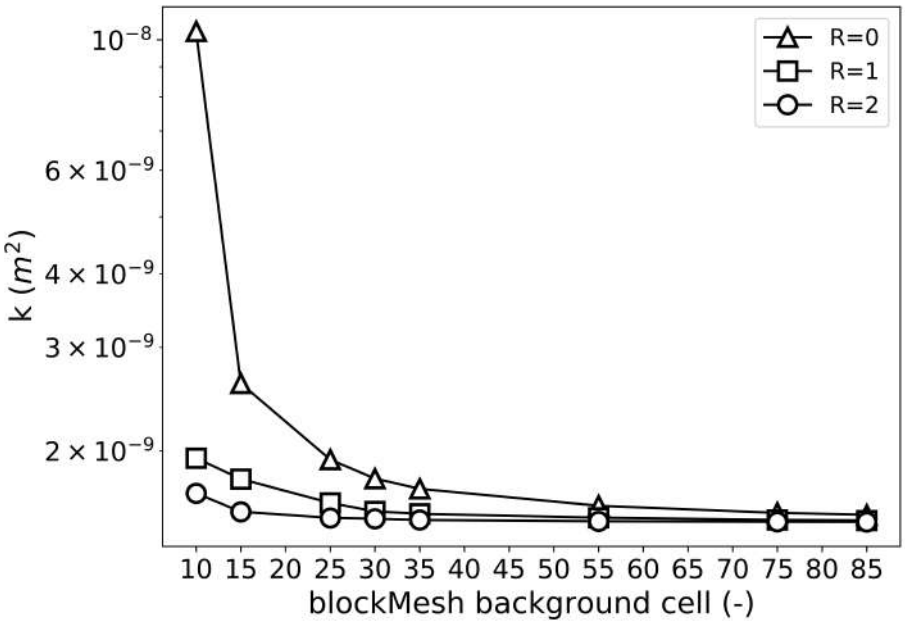

Figure 2: Values of calculated permeability with increasing overall mesh refinements expressed as number of background cells per equivalent pore diameter. Curves with different lines represent three different levels of mesh refinement close to the foam walls (R=0 means no refinement, R=2 means two subsequent refinements).

single-pore periodic geometry. The values of the subdivision of the initial bounding box considered were $C_{background} = \{10, 12, 15, 17, 20, 25, 30, 35, 45, 55, 75, 85\}$ and the values of the refinement level taken into account were $R = \{0, 1, 2\}$. The grid independence study, whose results are reported in Fig. 2 show the calculated value for the permeability k as a function of the `blockMesh` background cells number. For values of the refinement parameter $R > 1$ and for more than 25 background cells/pore the permeability reaches an asymptotic value. The best performance overall is achieved with R=2 because of the inferior wall-clock time for the solution to converge, indicating that a good trade off between accuracy and computational time could be achieved, with a number of subdivision ranging of 22. An additional grid independence investigation at different porosity values, $\varepsilon = \{0.77, 0.79, 0.85, 0.89, 0.95\}$ and $R = 2$, was carried out to ensure

that the accuracy of the solution, previously calculated, remained in the same range of error varying the porosity. Fig. 3, reporting the relative error with respect to the asymptotic value of the permeability, $e_r = |k_{as} - k|/k_{as}$, illustrate how the error lies below 2% except for the highest value of porosity ($\varepsilon = 95\%$), where it slightly depart from the other curves.

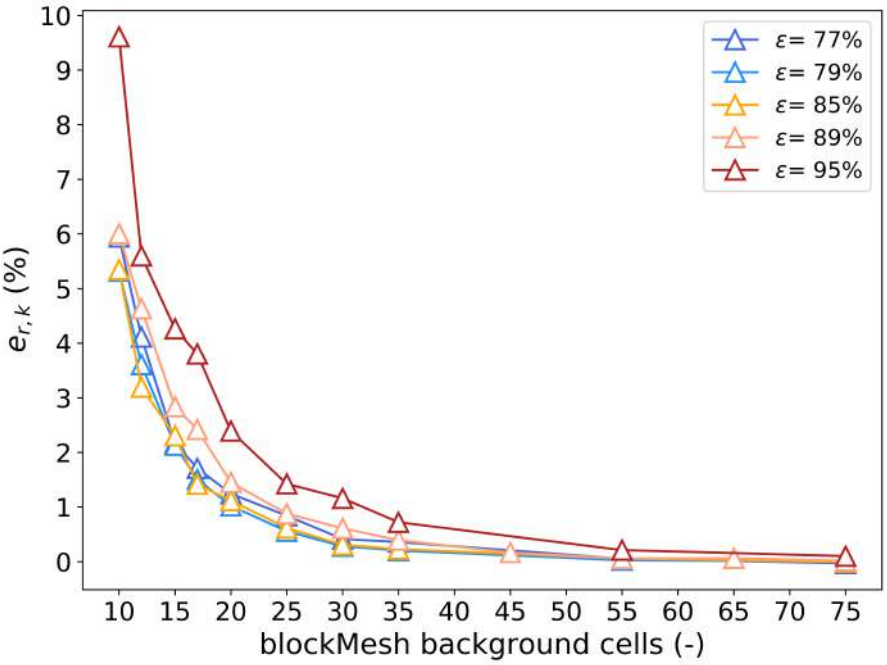

Figure 3: The relative error of the permeability e_r, for increasing overall mesh refinements, again expressed as number of background cells per equivalent pore diameter. Curves with different colors represent five different values of porosity $\varepsilon = \{77, 79, 85, 89, 95\}$

The results previously obtained were used to tune the meshing procedure for the randomly generated geometries. In particular, the aim was to determine the dimensions of the *Representative Elementary Volume* (REV), in terms of the number of foam pores contained. Flow field simulations were run on increasingly larger cubic portion of the same *monodisperse* foam, with sides respectively equal to the length of 2, 3, 4 and 5 pore diameters. The values of porosity ε, superficial porosity ε_s and permeability k were considered in order to determine

the optimal size of the computational domain. Following the meshing strategy exposed above, to generate the computational grid were used 20 mesh-cells per pore and R = 2, while the simulations were run at Re $= 1e-03$, in steady-state condition.

Pores/side	ε	ε_s	k (m^2)	$e_{r,k}$ (%)	Mesh Cells
2	0.900	0.878	3.24×10^{-9}	3.73	8.7×10^5
3	0.908	0.903	3.53×10^{-9}	5.01	2.8×10^6
4	0.902	0.917	3.32×10^{-9}	1.26	6.7×10^6
5	0.905	0.893	3.36×10^{-9}	0.00	1.3×10^7

Table 1: The results of computational domain dimension study carried out increasing progressively the dimensions of the computational domain. Along with the number of mesh cells, the table reports the calculated values for the porosity ε, the superficial porosity ε_s, permeability k and the error $e_{r,k}$ with respect to the most accurate case (5 pores/side)

The results are reported in Tab. 1. Considering the rapidly increasing computational costs and the small incremental geometrical differences between the two bigger computational domains, the choice was made to consider a cubic foam portion whose side equals four equivalent pore diameters to be a representative elementary volume for the cases considered in this work.

Finally, a grid independence study was also carried out for the scalar transport cases. The value used to compare the results was the scalar total flux, defined as $F_{tot} = F_{tot}^{in} - F_{tot}^{out}$. These simulations were run, again, on the Kelvin's Cell geometry, considering the same range of subdivision $C_{background}$ as previously mentioned, with a refinement level R = 2. The operating condition used were Re $= 1e-03$, Pe = 50, in steady-state conditions. The simulations were carried out for a high value of porosity, $\varepsilon = 0.89$,in order to account for effects on the colloidal deposition due to the great void fraction of the system. The plot in Fig. 4 show the error relative to the asymptotic value, $e_{r,F} = |F_{tot}^{as} - F_{tot}|/F_{tot}^{as}$, as parameter for comparison between the different meshes, in analogy to the momentum transport study.

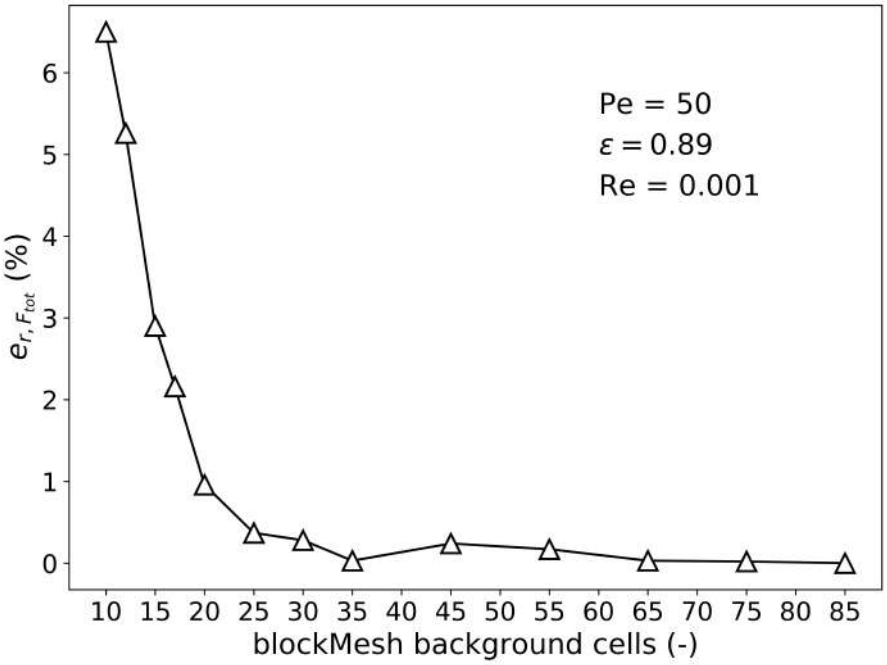

Figure 4: The relative error of the total flux F_{tot}, e_r, for increasing overall mesh refinements.

The results showed that 20 cells per pore were an adequate trade off to describe scalar transport phenomena, with an error with respect to the asymptotic value $e_r \approx 1\%$. Therefore, for grid independent simulations on a computational domain representing a REV for the considered foams, this would results in meshes size of approximately eight to nine million cells.

4.2. Numerical analysis

An example of the flow field simulations is reported in Fig. 5 for the case of 30 PPI and porosity $\varepsilon = 85\%$. The results for the permeability k, reported in Fig. 7, confirm the fact that the higher the porosity, the higher the permeability, which instead decreases rapidly with increasing PPI. Moreover the histogram show how the poly-disperse cases systematically present a higher permeability with respect to more ideal cases such as Kelvin's Cell or mono-disperse foams.

A global overview of the simulations and geometry is illustrated in Fig. 6

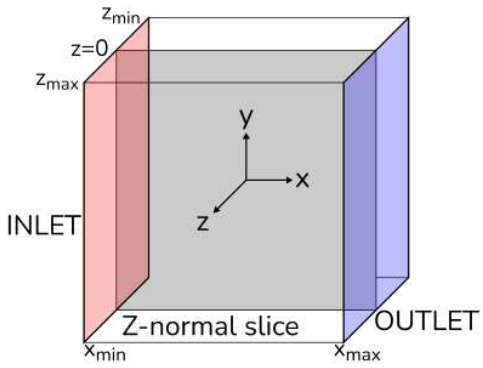

(a) z-normal slicing plane location

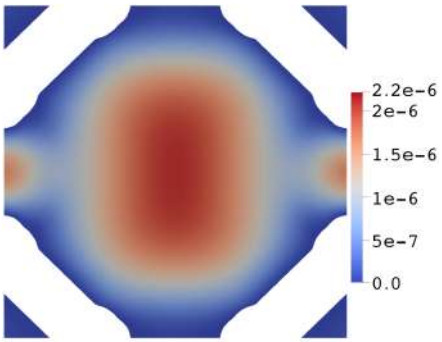

(b) KC

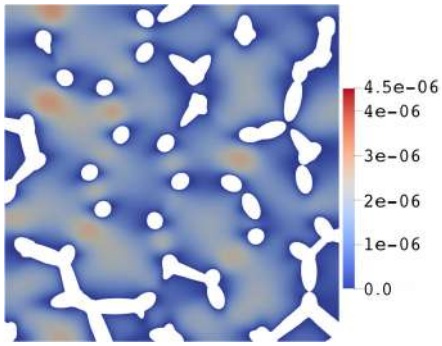

(c) MONO

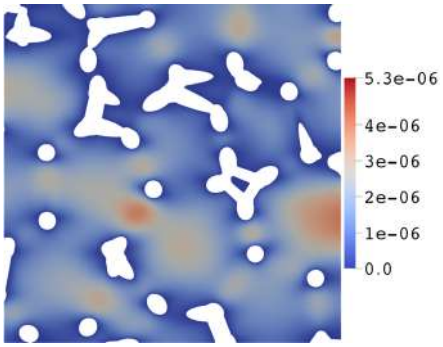

(d) CV = 0.2

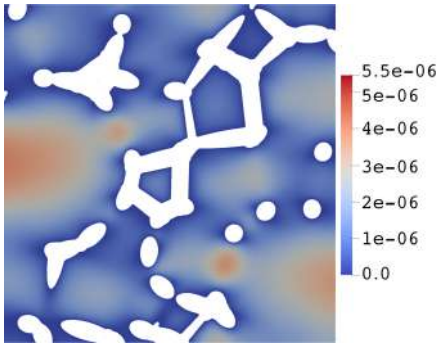

(e) CV = 0.35

Figure 5: Contour plots of the velocity magnitude U (m/s) for the four different geometrical models (30 PPI and $\varepsilon = 85\%$). In (a) an exemplification of the computational domain is reported in order to show the location of the z-normal slicing plane (at coordinate z = 0) used to extract the following contours: (b) Kelvin's Cell, (c) mono-disperse Voronoi, (d) poly-disperse Voronoi-Laguerre with CV = 0.2, (e) poly-disperse Voronoi-Laguerre with CV = 0.35

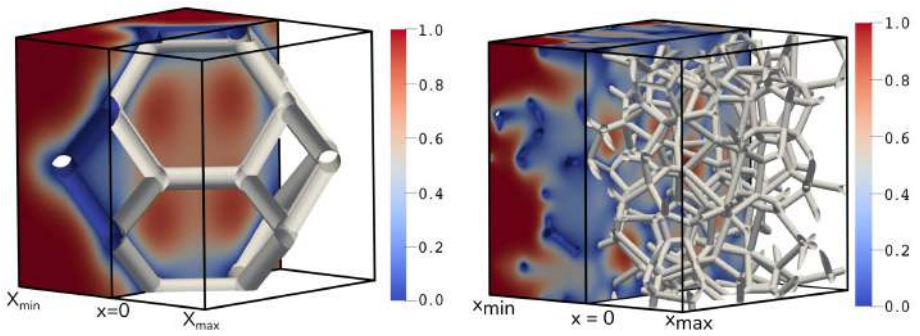

(a) KC (b) Voronoi-Laguerre

Figure 6: Contour plots of normalized concentration C for foams with 30 PPI and ε = 95%: (a) Kelvin's Cell, (b) poly-disperse Voronoi-Laguerre with CV = 0.35. The slicing plane is at x = 0

where there are reported and example of `scalartTransportFoam` solution together with foam solid structure.

From the scalar transport simulations a macroscopic measure of the filtration efficiency can be obtained. An example of the solution of the simulations is reported in the contour plot of Fig. 8 for the case of 30 PPI and porosity ε = 85%. Fig. 9 shows the relationship between the advective Damköhler number Da, defined in Eq. (13), as a function of the Péclet number.

In particular, Da number is reported for the all values of PPI (10, 20, 30, 45) as well as for different geometrical models. However, it can be noticed that keeping constant the Pe value and the geometry model, the Da values for different PPI collapse to the same point. This comes from the fact that the Damköhler number normalizes the deposition rate with respect to the dimension of the computational domain and that in laminar regime these cases are proportionally scaled. Globally, at increasing Pe number, the quantity of colloids impacting on the solid surface of the foam decreases following a power law, which was expected to some extent, considering the results of previous studies (Yao et al., 1971) on Brownian clean-bed filtration. At Pe $>$ 100, the difference between the different geometrical models is very small. This comes from the

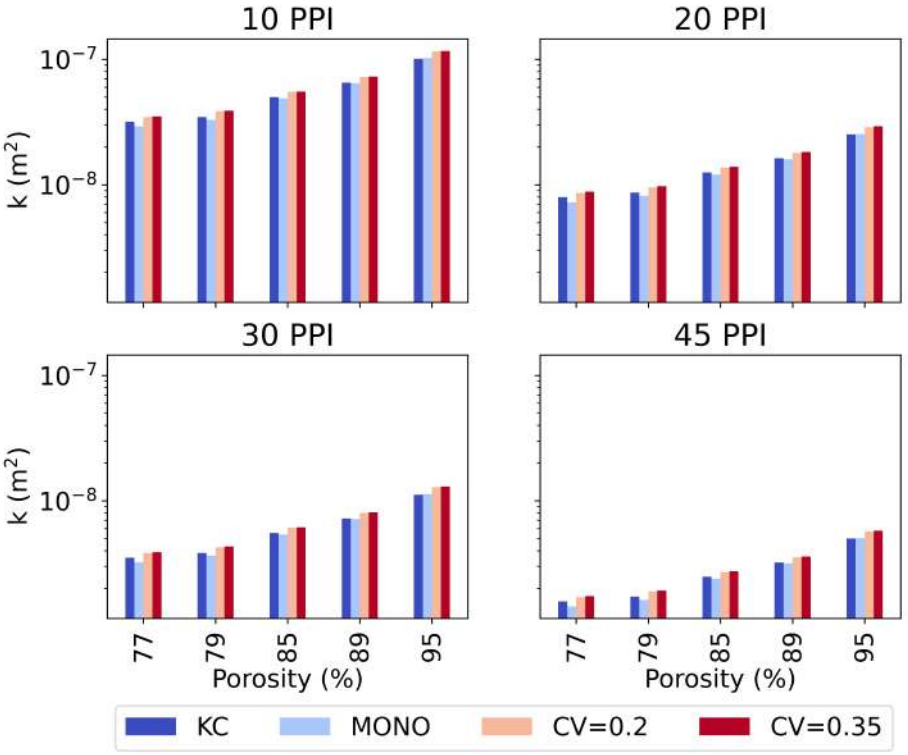

Figure 7: Permeability k vs. porosity, with each subplot representing the results for the four different values of PPI. Different colors represent a different geometry: Kelvin's Cell, mono-disperse Voronoi and poly-disperse Voronoi-Laguerre foams with different coefficient of variation. For an effective interpretation of this bar plot, the reader is advised to refer to the color version of this paper available online

fact that the corresponding colloidal particle size is closer to the micrometer and and the molecular diffusion coefficient becomes very small. At lower Pe number the difference between the four different model is not negligible and it should be investigated further. A new coefficient, $C_{KC} = \mathrm{Da}_{KC}/\mathrm{Da}_{VOR}$, the ratio between the Damköhler number obtained from the Kelvin's cell model and the ones derived from Voronoi tessellations, was introduced to more easily explore the effect of foam randomness specifically and also investigate the relationship with macro-scale parameters such as porosity ε, specific surface S_V and tortuosity τ. The latter defined as in Eq. (16):

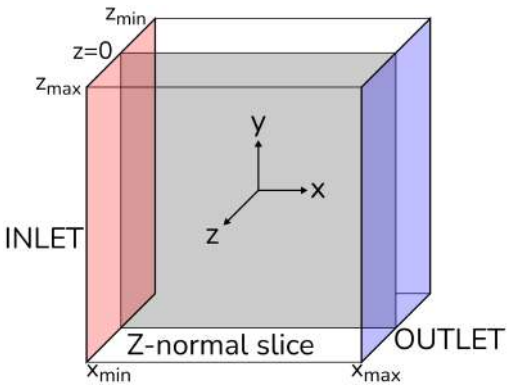

(a) z-normal slicing plane location

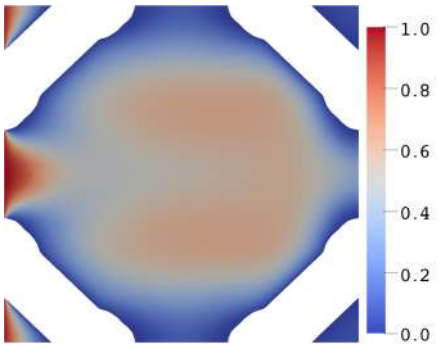

(b) KC

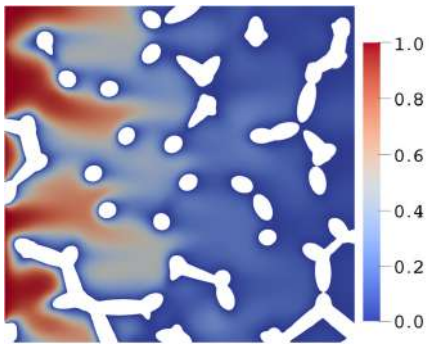

(c) MONO

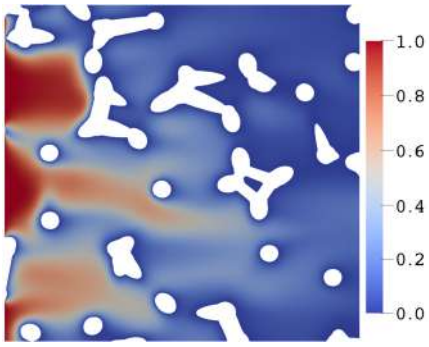

(d) CV = 0.2

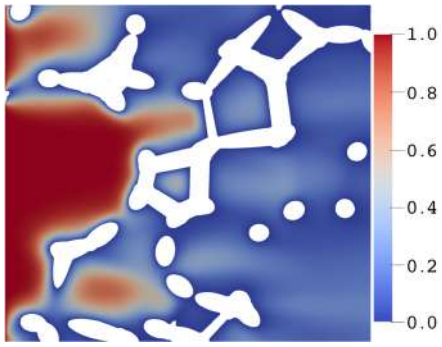

(e) CV = 0.35

Figure 8: Contour plots of the normalized concentration C for the four different geometrical models (30 PPI and $\varepsilon = 85\%$) In (a) an exemplification of the computational domain is reported in order to show the location of the z-normal slicing plane (at coordinate z = 0) used to extract the following contours: (b) Kelvin's Cell, (c) monodisperse Voronoi, (d) poly-disperse Voronoi-Laguerre with CV = 0.2, (e) poly-disperse Voronoi-Laguerre with CV = 0.35

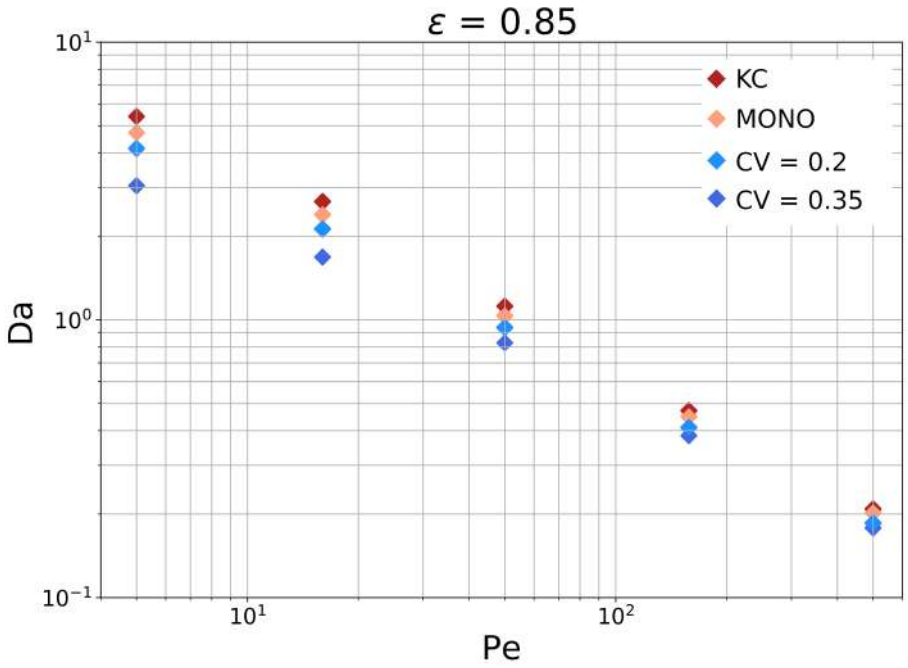

Figure 9: Particle deposition efficiency, as Da at constant porosity ($\varepsilon = 0.85$) for the four different geometries showing a power-law relationship between the Damköhler number and the Péclet number.

$$\tau = \frac{\int |\mathbf{U}| d\mathbf{x}}{\int U_x d\mathbf{x}} \tag{16}$$

where $\mathbf{U}$ is the local velocity vector and U_x is the local velocity component along the main flow direction (Koponen et al. 1996, Duda et al. 2011). The values of τ are reported in Fig. 12, which show how for such materials with very high void fraction and for the operating condition chosen, i.e. very low values of Re, the tortuosity depart slightly from unity.

A first approach was to try to interpret C_{KC} (which, for clarity, we remind the reader, it describes a particle deposition efficiency by means of a Damköler number) according to well known constitutive equations as function of the porosity, developed for fluid motion across solid obstacles, namely Happel (1958) for

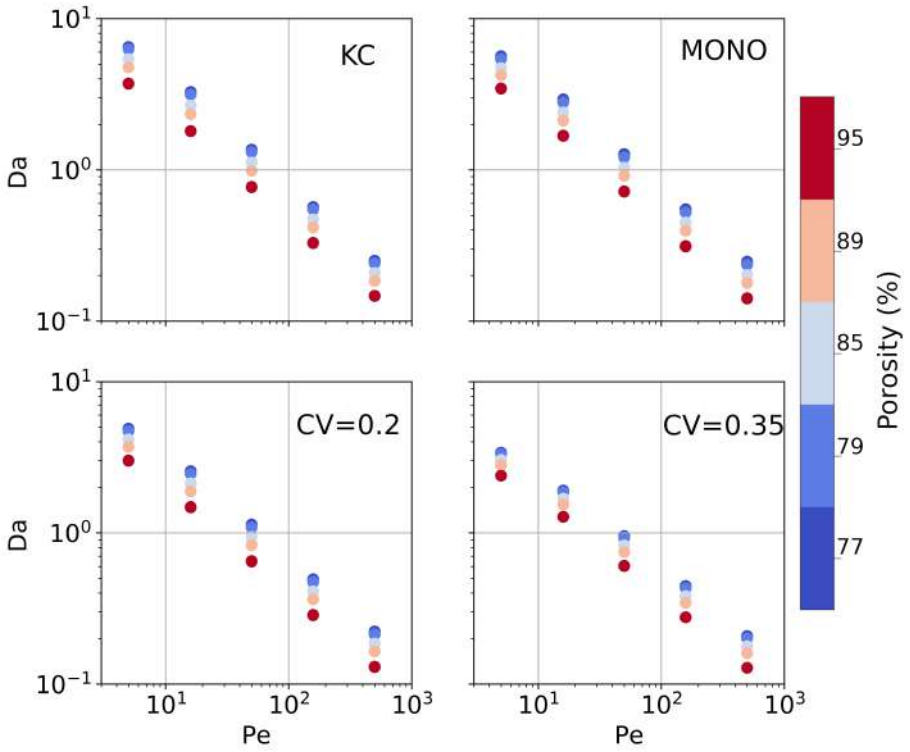

Figure 10: This figure highlights the effect of the porosity on the deposition efficiency: the rate of deposition decrease for the foam with higher porosity, regardless of the geometrical model.

spherical collectors and Kuwabara (1959) for cylindrical collectors [3]. The results of C_{KC}, as a function of Pe number, were normalized by the values of the cited functions, which depend on porosity. The results were then fitted according to a power law, in the form $f(\varepsilon, \mathrm{Pe}) = a \cdot \mathrm{Pe}^b$. This was done to ascertain if

[3]The two cited seminal papers, together with Levich (1962) mainly explored the fluid dynamic structure of flow past different arrangements of collectors. For the reader specifically interested in the evolution of different approaches in obtaining constitutive equations for particle deposition efficiency by implementing different simplified geometrical models, we point out to (among others): the already cited Yao et al. (1971), then Rajagopalan and Tien (1976), Logan et al. (1995), Tufenkji and Elimelech (2004), Ma and Johnson (2010), and Boccardo et al. (2018)

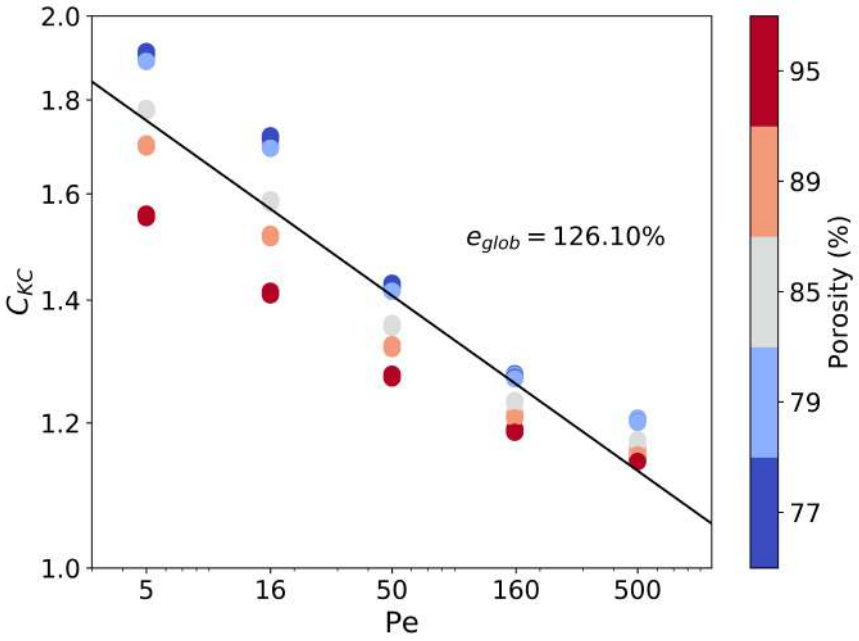

Figure 11: The Kelvin's Cell coefficient C_{KC}, as function of Pe, for the poly-disperse case: this geometry was generated from a sphere packing with a normal distribution of the mean sphere diameter and coefficient of variation $CV = 0.35$. The trend line of the data set and its global error are also reported.

these sole available relationships, which are capable of exactly predicting the impact of porosity on particle deposition for simplified geometries, can be used effectively for catalytic foams. However, this strategy didn't bring out any significant relationship, since the global relative error, calculated as the sum of the mean squared relative errors of the data with respect to the fitting at each Pe value, showed values well over 100%: for reference, if these correlations were able to perfectly describe the influence of porosity on particle deposition, the normalized results would collapse in a single Da-Pe power-law curve, reducing the error to zero. The underperformance of these analytical correlations was already highlighted by Boccardo et al. (2014) and while it was also expected in those cases (porous foams composed of cylindrical struts) for the "Happel"

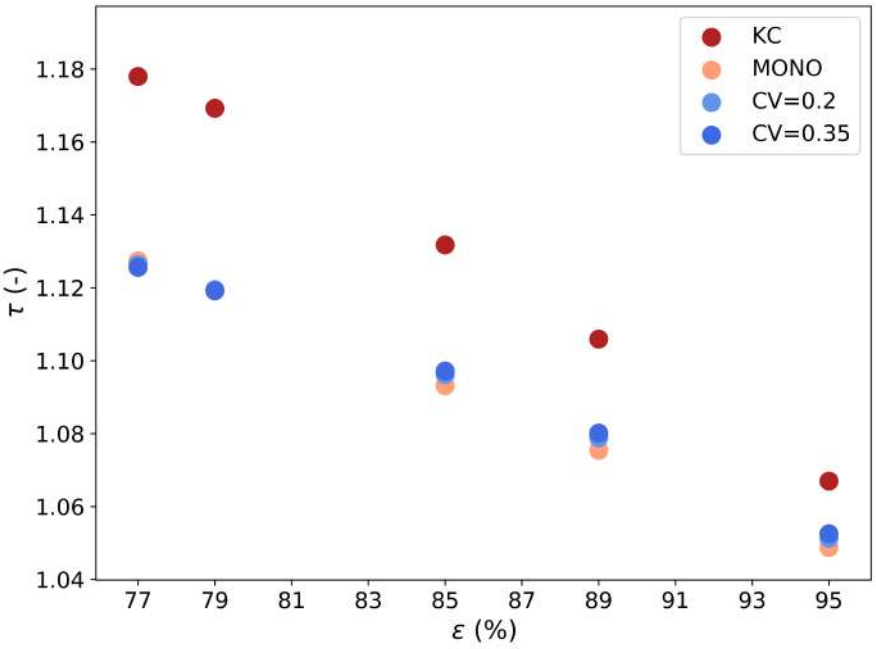

Figure 12: Tortuosity, calculated with Eq. (16): each series of colored points is the value ofτ calculated at different porosity ε for the four geometrical models (Kelvin's Cell, mono-disperse Voronoi, poly-disperse Voronoi-Laguerre with two different coefficient of variation.

model (developed for spheres arrangements), a better performance could be expected of the models based on the "Kuwabara" correlation (developed for arrangements of cylinders). Then, abandoning analytical but simplified correlations, a second approach was attempted trying to normalize the C_{KC} coefficient by adimensional numbers, i.e. ε, S_V and τ, all raised to the power of n, with the latter varying in the range $[-10; 10]$. Once again the results were fitted according to a power law model and the global error was calculated. Even so, no significant relationship could be obtained. A more detailed description of this analysis, along with the correlated plots can be found in the Supporting Information available with this article. Therefore, the results show how this kind of (usually employed) macroscopic geometric features are insufficient in explaining the variations in filtration performance, highlighting the need for more detailed

exploration using pore-scale simulations, the objective for which this workflow was developed. Moreoever, as it is shown in Boccardo et al. (2018) , the external boundary fluxes estimation have an important effect in the definition of effective parameters. In future works, more rigorous and precise definitions of the effective parameters will be considered (based for example on Municchi and Icardi (2020b)), studying more deeply the effect of the inlet (advective and diffusive) fluxes, and the asymptotic and pre-asymptotic flow and mass transfer upscaled regimes.

5. Conclusions

This work shows the features of an open-source workflow which is able to generate and characterize open-cell solid foams. This in-silico tool, developed with computer graphics software `Blender` and `Python` language scripting, gives the opportunity to use different models with growing complexity in terms of pore size distribution. The choice of models ranges from the ideal periodic Kelvin's cell to random foams generated with random weighted Voronoi tessellations and poly-disperse pore size distributions. These features give the user the possibility to use this tool to investigate several different morphologies and eventually optimize them, while the computational costs remain low. The geometries thus created have been used to perform CFD simulations, using the open-source code `OpenFOAM`, and later, as a test case, the event of an instantaneous superficial reaction/superficial deposition of colloidal particles, occurring on the solid surface, has also been investigated. The results obtained in this work by employing these models highlight that the macroscopic parameters, such as porosity, specific surface, or tortuosity alone are not enough to derive macroscopic relations to describe the particle deposition during early filtration; neither by using available and widely used (albeit simplified) analytical correlations, nor by developing new simple bespoke correlations based on these geometrical parameters. Thus, while we consider the value of the presented workflow to lie in the capacity for users to create numerical analysis campaigns

at a limited cost, in particular decreasing the overhead of the foam modeling, the study of the different geometrical models and their performance in terms of colloidal particles deposition is conceived as an example of the exploration capabilities of this workflow which we choose to limit to the work here presented. Future perspectives on this topic are then to further improve the understanding of the transport phenomena occurring inside these foams, by exploring *in-silico* a wider number of cases and especially by better discerning the geometrical peculiarities of each - beyond simple, and oft-used, descriptors like porosity or tortuosity. This motivates the choice of making the source code of this simulation platform, as well as the test cases for the simulations here presented, public and available to the community of researchers and practitioners, in order both to expand the technical capabilities of the workflow and increase the simulation data, which will prove invaluable in gaining a full understanding for these systems.

6. Declaration of Competing interest

The authors declare that they have no known competing financial interests or personal relationships that could have appeared to influence the work reported in this paper.

7. Acknowledgements

Computational resources were provided by HPC@POLITO, a project of Academic Computing within the Department of Control and Computer Engineering at the Politecnico di Torino (http://www.hpc.polito. it). We also acknowledge the CINECA award under the ISCRA initiative, for the availability of high performance computing resources and support. The Authors want to thank Matteo Icardi for the interesting discussions.

References

Agostini, E., 2021. Cefocat-public. https://github.com/mulmopro/CeFoCat-public.

Ambrosetti, M., Bracconi, M., Groppi, G., Tronconi, E., 2017. Analytical Geometrical Model of Open Cell Foams with Detailed Description of Strut-Node Intersection. Chemie-Ingenieur-Technik 89, 915–925. doi:10.1002/cite.201600173.

Aurenhammer, F., 1987. Power diagrams: properties, algorithms and. SIAM J. COMPUT. 16, 78–96.

Bensaid, S., Marchisio, D.L., Fino, D., 2010. Numerical simulation of soot filtration and combustion within diesel particulate filters. Chemical Engineering Science 65, 357–363. URL: http://dx.doi.org/10.1016/j.ces.2009.06.051, doi:10.1016/j.ces.2009.06.051.

Boccardo, G., Augier, F., Haroun, Y., Ferré, D., Marchisio, D.L., 2015. Validation of a novel open-source work-flow for the simulation of packed-bed reactors. Chemical Engineering Journal 279, 809–820–820. URL: http://dx.doi.org/10.1016/j.cej.2015.05.032, doi:10.1016/j.cej.2015.05.032.

Boccardo, G., Crevacore, E., Sethi, R., Icardi, M., 2018. A robust upscaling of the effective particle deposition rate in porous media. Journal of Contaminant Hydrology 212, 3–13. URL: http://dx.doi.org/10.1016/j.jconhyd.2017.09.002, doi:10.1016/j.jconhyd.2017.09.002, arXiv:1702.04527.

Boccardo, G., Marchisio, D.L., Sethi, R., 2014. Microscale simulation of particle deposition in porous media. Journal of Colloid and Interface Science 417, 227–237. URL: http://dx.doi.org/10.1016/j.jcis.2013.11.007, doi:10.1016/j.jcis.2013.11.007.

Bracconi, M., Ambrosetti, M., Maestri, M., Groppi, G., Tronconi, E., 2017. A systematic procedure for the virtual reconstruction of open-cell foams. Chem-

ical Engineering Journal 315, 608–620. URL: http://dx.doi.org/10.1016/j.cej.2017.01.069, doi:10.1016/j.cej.2017.01.069.

Brakke, K.A., 1992. The surface evolver. Experiment. Math. 1, 141–165. URL: https://projecteuclid.org:443/euclid.em/1048709050.

Chandra, V., Das, S., Peters, E.A., Kuipers, J.A., 2019. Direct numerical simulation of hydrodynamic dispersion in open-cell solid foams. Chemical Engineering Journal 358, 1305–1323. URL: https://doi.org/10.1016/j.cej.2018.10.017, doi:10.1016/j.cej.2018.10.017.

Crevacore, E., Boccardo, G., Marchisio, D., Sethi, R., 2016. Microscale colloidal transport simulations for groundwater remediation. Chemical Engineering Transactions 47, 271–276.

Das, S., Deen, N.G., Kuipers, J.A., 2016. Direct numerical simulation for flow and heat transfer through random open-cell solid foams: Development of an IBM based CFD model. Catalysis Today 273, 140–150. URL: http://dx.doi.org/10.1016/j.cattod.2016.03.048, doi:10.1016/j.cattod.2016.03.048.

Das, S., Deen, N.G., Kuipers, J.A., 2017. Immersed boundary method (IBM) based direct numerical simulation of open-cell solid foams: Hydrodynamics. AIChE Journal 63, 1152–1173. doi:10.1002/aic.15487.

Das, S., Sneijders, S., Deen, N.G., Kuipers, J.A., 2018. Drag and heat transfer closures for realistic numerically generated random open-cell solid foams using an immersed boundary method. Chemical Engineering Science 183, 260–274. doi:10.1016/j.ces.2018.03.022.

Della Torre, A., Lucci, F., Montenegro, G., Onorati, A., Dimopoulos Eggenschwiler, P., Tronconi, E., Groppi, G., 2016. CFD modeling of catalytic reactions in open-cell foam substrates. Computers and Chemical Engineering 92, 55–63. URL: http://dx.doi.org/10.1016/j.compchemeng.2016.04.031, doi:10.1016/j.compchemeng.2016.04.031.

Della Torre, A., Montenegro, G., Tabor, G.R., Wears, M.L., 2014. CFD characterization of flow regimes inside open cell foam substrates. International Journal of Heat and Fluid Flow 50, 72–82. URL: http://dx.doi.org/10.1016/j.ijheatfluidflow.2014.05.005, doi:10.1016/j.ijheatfluidflow.2014.05.005.

Duda, A., Koza, Z., Matyka, M., 2011. Hydraulic tortuosity in arbitrary porous media flow. Phys. Rev. E 84, 036319. URL: https://link.aps.org/doi/10.1103/PhysRevE.84.036319, doi:10.1103/PhysRevE.84.036319.

Gostik, J., 2017. Add an 'edges' attribute to Voronoi objects? #7103. URL: https://cutt.ly/voronoi-edges.

Habisreuther, P., Djordjevic, N., Zarzalis, N., 2009. Statistical distribution of residence time and tortuosity of flow through open-cell foams. Chemical Engineering Science 64, 4943–4954. URL: http://dx.doi.org/10.1016/j.ces.2009.07.033, doi:10.1016/j.ces.2009.07.033.

Happel, J., 1958. Viscous flow in multiparticle systems: slow motion of fluids relative to beds of spherical particles. AIChE journal 4, 197–201.

Icardi, M., Boccardo, G., Marchisio, D.L., Tosco, T., Sethi, R., 2014. Pore-scale simulation of fuid flow and solute dispersion in three-dimensiona porous media. Engineering Sciences and Fundamentals 2014 - Core Programming Area at the 2014 AIChE Annual Meeting 2, 725. doi:10.1103/PhysRevE.90.013032.

Inayat, A., Freund, H., Schwab, A., Zeiser, T., Schwieger, W., 2011a. Predicting the specific surface area and pressure drop of reticulated ceramic foams used as catalyst support. Advanced Engineering Materials 13, 990–995. doi:10.1002/adem.201100038.

Inayat, A., Freund, H., Zeiser, T., Schwieger, W., 2011b. Determining the specific surface area of ceramic foams: The tetrakaidecahedra model revisited.

Chemical Engineering Science 66, 1179–1188. doi:10.1016/j.ces.2010.12.031.

Inayat, A., Schwerdtfeger, J., Freund, H., Körner, C., Singer, R.F., Schwieger, W., 2011c. Periodic open-cell foams: Pressure drop measurements and modeling of an ideal tetrakaidecahedra packing. Chemical Engineering Science 66, 2758–2763. doi:10.1016/j.ces.2011.03.031.

Incera Garrido, G., Patcas, F.C., Lang, S., Kraushaar-Czarnetzki, B., 2008. Mass transfer and pressure drop in ceramic foams: A description for different pore sizes and porosities. Chemical Engineering Science 63, 5202–5217. doi:10.1016/j.ces.2008.06.015.

Karimi, M., Droghetti, H., Marchisio, D., 2017. Pufoam : A novel open-source cfd solver for the simulation of polyurethane foams. Computer Physics Communications 217, 138–148. URL: https://www.sciencedirect.com/science/article/pii/S0010465517300978, doi:https://doi.org/10.1016/j.cpc.2017.03.010.

Kloss, C., Goniva, C., Hager, A., Amberger, S., Pirker, S., 2012. Models, algorithms and validation for opensource dem and cfd-dem. Progress in Computational Fluid Dynamics 12, 140 – 152. doi:10.1504/PCFD.2012.047457.

Koponen, A., Kataja, M., Timonen, J., 1996. Tortuous flow in porous media. Phys. Rev. E 54, 406–410. URL: https://link.aps.org/doi/10.1103/PhysRevE.54.406, doi:10.1103/PhysRevE.54.406.

Krishnan, S., Murthy, J.Y., Garimella, S.V., 2006. Direct Simulation of Transport in Open-Cell Metal Foam. Journal of Heat Transfer 128, 793. doi:10.1115/1.2227038.

Kumar, P., Topin, F., 2014. The geometric and thermohydraulic characterization of ceramic foams: An analytical approach. Acta Materialia 75, 273–286. URL: http://dx.doi.org/10.1016/j.actamat.2014.04.061, doi:10.1016/j.actamat.2014.04.061.

Kuwabara, S., 1959. The forces experienced by randomly distributed parallel circular cylinders or spheres in a viscous flow at small reynolds numbers. Journal of the physical society of Japan 14, 527–532.

König, R., Spaggiari, M., Santoliquido, O., Principi, P., Bianchi, G., Ortona, A., 2020. Micropollutant adsorption from water with engineered porous ceramic architectures produced by additive manufacturing and coated with natural zeolite. Journal of Cleaner Production 258, 120500. URL: https://www.sciencedirect.com/science/article/pii/S0959652620305473, doi:https://doi.org/10.1016/j.jclepro.2020.120500.

Lacroix, M., Nguyen, P., Schweich, D., Pham Huu, C., Savin-Poncet, S., Edouard, D., 2007. Pressure drop measurements and modeling on SiC foams. Chemical Engineering Science 62, 3259–3267. doi:10.1016/j.ces.2007.03.027.

Lautensack, C., Giertzsch, M., Godehardt, M., Schladitz, K., 2008. Modelling a ceramic foam using locally adaptable morphology. Journal of Microscopy 230, 396–404. doi:10.1111/j.1365-2818.2008.01998.x.

Levich, V.G., 1962. Physicochemical hydrodynamics .

Logan, B.E., Jewett, D., Arnold, R.G., Bouwer, E., O'Melia, C., 1995. Clarification of clean-bed filtration models. Journal of environmental engineering 121, 869–873.

Lucci, F., Della Torre, A., Montenegro, G., Dimopoulos Eggenschwiler, P., 2015. On the catalytic performance of open cell structures versus honeycombs. Chemical Engineering Journal 264, 514–521. URL: http://dx.doi.org/10.1016/j.cej.2014.11.080, doi:10.1016/j.cej.2014.11.080.

Lucci, F., Della Torre, A., Montenegro, G., Kaufmann, R., Dimopoulos Eggenschwiler, P., 2017. Comparison of geometrical, momentum and mass transfer characteristics of real foams to Kelvin cell lattices for catalyst applications. International Journal of Heat and Mass Transfer 108, 341–350. URL: http:

//dx.doi.org/10.1016/j.ijheatmasstransfer.2016.11.073https://linkinghub.elsevier.com/retrieve/pii/S0017931016325674, doi:10.1016/j.ijheatmasstransfer.2016.11.073.

Lucci, F., Della Torre, A., von Rickenbach, J., Montenegro, G., Poulikakos, D., Dimopoulos Eggenschwiler, P., 2014. Performance of randomized Kelvin cell structures as catalytic substrates: Mass-transfer based analysis. Chemical Engineering Science 112, 143–151. URL: http://dx.doi.org/10.1016/j.ces.2014.03.023, doi:10.1016/j.ces.2014.03.023.

Ma, H., Johnson, W.P., 2010. Colloid retention in porous media of various porosities: Predictions by the hemispheres-in-cell model. Langmuir 26, 1680–1687.

Marcato, A., Boccardo, G., Marchisio, D., 2021. A computational workflow to study particle transport and filtration in porous media: Coupling cfd and deep learning. Chemical Engineering Journal 417, 128936. URL: https://www.sciencedirect.com/science/article/pii/S1385894721005295, doi:https://doi.org/10.1016/j.cej.2021.128936.

Meloni, E., Caldera, M., Palma, V., Pignatelli, V., Gerardi, V., 2019. Soot abatement from biomass boilers by means of open-cell foams filters. Renewable Energy doi:10.1016/j.renene.2018.07.098.

Municchi, F., Icardi, M., 2020a. Generalized multirate models for conjugate transfer in heterogeneous materials. Physical Review Research 2, 013041.

Municchi, F., Icardi, M., 2020b. Macroscopic models for filtration and heterogeneous reactions in porous media. Advances in Water Resources 141, 103605.

Nie, Z., Lin, Y., Tong, Q., 2017a. Modeling structures of open cell foams. Computational Materials Science 131, 160–169. URL: http://dx.doi.org/10.1016/j.commatsci.2017.01.029, doi:10.1016/j.commatsci.2017.01.029.

Nie, Z., Lin, Y., Tong, Q., 2017b. Numerical investigation of pressure drop and heat transfer through open cell foams with 3D Laguerre-Voronoi

model. International Journal of Heat and Mass Transfer 113, 819–839. URL: http://dx.doi.org/10.1016/j.ijheatmasstransfer.2017.05.119, doi:10.1016/j.ijheatmasstransfer.2017.05.119.

Rajagopalan, R., Tien, C., 1976. Trajectory analysis of deep-bed filtration with the sphere-in-cell porous media model. AIChE Journal 22, 523–533.

Redenbach, C., 2009. Microstructure models for cellular materials. Computational Materials Science doi:10.1016/j.commatsci.2008.09.018.

Richardson, J.T., Remue, D., Hung, J.K., 2003. Properties of ceramic foam catalyst supports: Mass and heat transfer. Applied Catalysis A: General 250, 319–329. doi:10.1016/S0926-860X(03)00287-4.

Rycroft, C.H., 2009. VORO++: A three-dimensional Voronoi cell library in C++. Chaos 19, 1–14. doi:10.1063/1.3215722.

Singh, S., Bhatnagar, N., 2018. A survey of fabrication and application of metallic foams (1925–2017). Journal of Porous Materials 25, 537–554. doi:10.1007/s10934-017-0467-1.

Smith, W., 2019. Tess: A 3D cell-based Voronoi Python library based on voro++. URL: https://github.com/wackywendell/tess.

Sullivan, R.M., Ghosn, L.J., Lerch, B.A., 2008. A general tetrakaidecahedron model for open-celled foams. International Journal of Solids and Structures doi:10.1016/j.ijsolstr.2007.10.028.

Thomson, W., et al., 1887. On the division of space with minimum partitional area. Acta mathematica 11, 121–134.

Tosco, T., Bosch, J., Meckenstock, R.U., Sethi, R., 2012. Transport of ferrihydrite nanoparticles in saturated porous media: role of ionic strength and flow rate. Environmental science & technology 46, 4008–4015.

Tufenkji, N., Elimelech, M., 2004. Correlation equation for predicting single-collector efficiency in physicochemical filtration in saturated porous media. Environmental science & technology 38, 529–536.

Twigg, M.V., Richardson, J.T., 2007. Fundamentals and applications of structured ceramic foam catalysts. Industrial and Engineering Chemistry Research 46, 4166–4177. doi:10.1021/ie061122o.

Wehinger, G.D., Kolaczkowski, S.T., Schmalhorst, L., Beton, D., Torkuhl, L., 2019. Modeling fixed-bed reactors from metal-foam pellets with detailed CFD. Chemical Engineering Journal 373, 709–719. URL: https://linkinghub.elsevier.com/retrieve/pii/S1385894719310873, doi:10.1016/j.cej.2019.05.067.

Wejrzanowski, T., Skibinski, J., Szumbarski, J., Kurzydlowski, K.J., 2013. Structure of foams modeled by Laguerre-Voronoi tessellations. Computational Materials Science 67, 216–221. URL: http://dx.doi.org/10.1016/j.commatsci.2012.08.046, doi:10.1016/j.commatsci.2012.08.046.

Whitaker, S., 2013. The method of volume averaging. volume 13. Springer Science & Business Media.

Yao, K.M., Habibian, M.T., O'Melia, C.R., 1971. Water and waste water filtration. concepts and applications. Environmental science & technology 5, 1105–1112.